Invasion percolation in a hydrostatic or permeability gradient: Experiments and simulations

M. Chaouche, N. Rakotomalala, and D. Salin
Laboratoire d'Acoustique et Optique de la Matière Condensée, Université Pierre et Marie Curie, Tour 13, Boite 78, 75252 Paris Cedex 05, France

B. Xu and Y. C. Yortsos
Department of Chemical Engineering and Petroleum Engineering Program, University of Southern California, Los Angeles, California 90089-1211

(Received 18 October 1993)

We present experiments and simulations of slow drainage in three-dimensional (3D) porous media, either homogeneous and in the presence of gravity or heterogeneous and in its absence. An acoustic technique allows for an accurate study of the 3D fronts and the crossover region. Our results suggest that both cases can be described by invasion percolation in a gradient. For the case of gravity, the front tail width scales with the Bond number as $\sigma_{FT} \sim B^{-0.47}$, in agreement with the theory. For the case of permeability gradient a different scaling is found, in agreement with a modified theory of gradient percolation developed here.

PACS number(s): 47.55.Mh, 05.40.+j, 47.55.Kf

I. INTRODUCTION

Important in oil recovery, hydrology, and chemical engineering, immiscible displacement in porous media finds as much interest in the physics of disordered media. The front between two immiscible fluids exhibits characteristic patterns depending on the displacement process [1]. Well studied is the constant rate displacement in a porous medium of a wetting fluid, which initially occupies the medium, by a nonwetting fluid. This process is known as *drainage*. The reverse process, where a wetting fluid displaces a nonwetting fluid, is termed *imbibition*. In this paper, we are strictly concerned with drainage, the pore-level mechanics of which are well understood. For example, fast, viscous-dominated displacement in the limit of large viscosity ratio (viscous fingering) is modeled by diffusion-limited aggregation [2]. Invasion percolation (IP) [3] describes the opposite extreme of slow displacements, where capillary forces dominate over viscous and lead to percolation patterns [4]. In the absence of pressure gradients, the latter have the fractal properties, including the critical exponents, of ordinary percolation. For example, the displacing front has the geometry of the incipient percolation cluster, which is a self-similar fractal object of a specified fractal dimension.

For these regimes to apply requires macroscopically homogeneous media in the absence of external forces. However, this is not the case in many practical applications. For example, in a vertical displacement involving fluids of different densities, gravity competes with capillary and viscous forces by exerting hydrostatic pressure gradients. The gravity number (also called the Bond number) $B_g = \Delta\rho g_x \bar{r}^2/\gamma$ measures the competition between gravity and capillary forces. Here $\Delta\rho$ denotes the difference between the density of wetting and nonwetting fluids, g_x is the acceleration of gravity in the flow direction x, $\bar{r}$ is the mean pore size, and γ is the interfacial tension. If the displacement is downdip (injection of the lighter fluid from the top, $B_g > 0$), gravity acts to limit the fractal regime to a finite extent and the front becomes self-affine. Its extent is measured by the front width σ in two dimensions or by the front-tail width σ_{FT} in three-dimensional (3D) geometries. Either obeys a scaling law with the Bond number, as shown below. A compact pattern follows the fractal front. The opposite case, where the displacement is updip (injection of the lighter fluid from the bottom, $B_g < 0$), leads to gravity fingering [6]. Gravity effects for the stable case ($B_g > 0$) have been modeled with gradient percolation [7,8] (GP) and with invasion percolation in a gradient [5] (IPG), which are modified versions of ordinary and invasion percolation, respectively. Experimental confirmation of the theory has been obtained for drainage in 2D geometries [9]. However, no experimental confirmation exists so far for 3D displacements, where only one B_g value has been tested [5].

Another external force that may also act in a similar fashion arises from heterogeneity. Recent work [10] on immiscible displacement in heterogeneous porous media has indicated that spatial permeability variations also act in ways similar to gravity, with the additional feature that contrary to gravity, permeability gradients may vary in space. For example, consider drainage in a horizontal medium with a permeability gradient. Because the nonwetting fluid preferably penetrates the high permeability regions, we expect that a form of gradient percolation would also describe this process, but with a different number B_k, now based on the permeability gradient. We shall call B_k the *heterogeneity* Bond number. In this paper, we postulate that both these effects (gravity and permeability heterogeneity) can be described by IPG. We present three-dimensional experiments in bead packs and pore network simulations to test this conjecture for gravity and permeability heterogeneity.

II. PRELIMINARIES

Before we proceed, we summarize briefly what is known about gradient percolation in the present context. We recall that GP is a lattice percolation process, where the occupation probability p is not constant, but decreases (typically linearly) with one of the lattice coordinates [5,7,8]. IPG is the analog of this process to invasion percolation. Invasion percolation in a hydrostatic pressure gradient was first proposed by Wilkinson [7] to describe imbibition in the presence of gravity. Sapoval and co-workers [8] considered a more general problem involving diffusion. In both applications, however, the percolation (occupation) probability $p(x)$ is spatially varying. In the case of drainage at low rates, of interest to this paper, p is related to the capillary pressure Π, which denotes the difference between the pressure of nonwetting and wetting fluids across an interface at the pore throat of size r, by the two relations

$$p=\int_r^\infty \alpha(r)dr \tag{1}$$

and

$$\Pi=2\gamma/r\ , \tag{2}$$

where $\alpha(r)$ is the pore size distribution. In the absence of gradients, the fluid displacement is described by IP, where p is uniform in space, the front has the fractal structure of the percolation cluster, and its extent is given by the correlation length ξ, which satisfies the percolation scaling [4] $\xi\sim l|p-p_c|^{-\nu}$. Here l is the lattice spacing, the correlation exponent is $\nu=\frac{4}{3}$ or 0.88, in 2D or 3D, respectively, and p_c is the bond percolation threshold, which is a lattice property (e.g., $p_c\approx 0.25$ for a simple cubic lattice in bond percolation). The displacement is driven by an increase in Π and reaches breakthrough ($\xi\gg l$) when p reaches p_c, in which case Π attains its capillary threshold value Π_c.

In the presence of gradients (e.g., along the direction x), the displacement process is described by IPG, where now p is continuously decreasing. A front location $x_c(t)$, where $p(x_c)=p_c$, can be identified. Clearly, this front location $x_c(t)$ varies with time as a result of the imposed pressure difference $P(t)$, which must increase for the displacement to proceed [e.g., $P(t)=\Pi_c+\Delta\rho g_x x_c(t)$ for the case of gravity]. The vicinity of x_c is a crossover region, described by the theory of finite size effects in percolation [4]. In both GP and IPG, there is a region around x_c of finite extent σ where percolation theory applies. Its scaling is given by [7,8]

$$\frac{\sigma}{l}\sim|l\nabla p|^{-\nu/(1+\nu)}\ , \tag{3}$$

where σ indicates the front width in 2D or the front-tail width [8] σ_{FT} in 3D. The difference in the definition of the front extent in 2D and 3D geometries reflects the different connectivity properties in the respective dimensions [8].

In the stable case (negative values of dp/dx), the theory of IPG allows for the invading fluid concentration $S_0(x)$ to be determined through the relationship [8]

$$S_0\sim p(\delta p)^\beta\Pi_f\left(\frac{x_c-x}{\sigma}\right)\ , \tag{4}$$

where the relation $(p-p_c)/\delta p=(x_c-x)/\sigma$ was implied, $\delta p\equiv|\nabla p|^{1/1+\nu}$, $\beta=0.45$ in 3D, and the scaling function Π_f was computed in Ref. [8]. The function Π_f is unique to the GP process. It accounts for the fractal nature of the front in the vicinity of p_c as well as for the approach to a compact pattern away from the front (near the inlet), where the invading saturation is described by the expression $S_0\sim(x_c-x)^\beta$. A schematic of this function, computed from gradient percolation in a 3D lattice, is shown in Fig. 1.

Consider now the application of the above to gravity or permeability gradients. In either case, the link of the probability gradient to the Bond number is through the previous capillary pressure relationship. We take for simplicity a uniform pore-size distribution $\alpha(r)$ of width λ and mean pore size $\bar r$, from which it readily follows that $p=(\bar r-r)/\lambda+\frac{1}{2}$. In the case of gravity only, the capillary pressure varies in both space and time, $\Pi=P(t)-\Delta\rho g x$, but $\bar r$ is fixed. Thus $dp/dx=-\Delta\rho g r^2/2\gamma\lambda$. Evaluating near the front gives

$$dp/dx|_c=-B_g(r_c^2/2\lambda\bar r^2)\ , \tag{5}$$

where r_c corresponds to p_c. In the case of heterogeneity only, the capillary pressure is uniform in space but variable in time, thus

$$dp/dx=(1/\lambda)(d\bar r/dx)=-(1/\lambda)B_k\ , \tag{6}$$

where $B_k\equiv-d\bar r/dx\sim-d\sqrt{k}/dx$. If the permeability k is decreasing in the direction of the displacement ($B_k>0$), invasion by the nonwetting fluid requires higher pressures, the permeability gradient acting to stabilize the front. In the opposite case ($B_k<0$) invasion is facilitated, leading to fingering due to capillary heterogeneity (which differs from the classical viscous fingering problem). Assuming that the lattice is of fixed spacing l, we shall have

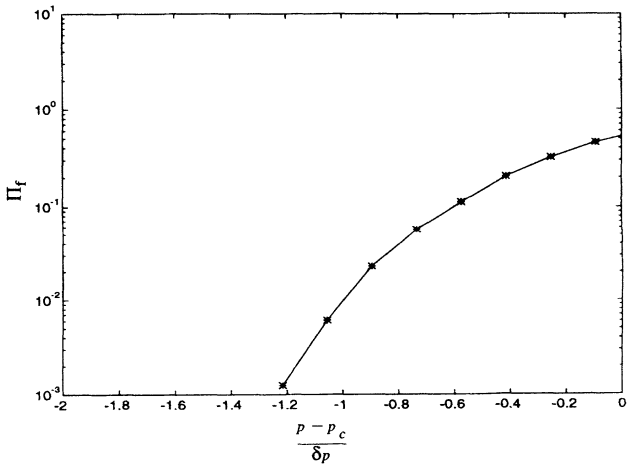

FIG. 1. The scaling function Π_f computed from gradient percolation in a 3D $348\times348\times50$ lattice.

$$\frac{\sigma}{l} \sim B^{-\nu/1+\nu} \tag{7}$$

for either the gravity or the permeability cases.

The condition of uniform spacing is necessary for (7) to be valid. However, in our experiments it was satisfied only in the gravity experiments. In the heterogeneity experiments, the permeability gradient was generated by a constant gradient in the bead size, which in turn imposed a gradient in the lattice spacing, since spacing and pore size in a bead pack are proportionally related ($l \sim a\bar{r}$). Under such conditions, Eq. (7) should not be applicable, in fact the front width should be a function of time (or of x_c), decreasing with x_c in the case $B_k > 0$. A modification of the IPG to model this situation is necessary and such is proposed below. Before we proceed, we present the experimental results.

III. EXPERIMENTS

The experiments were performed with porous media consisting of packed glass beads, the diameter of which ranged between 80 μm and 1 mm. For the gravity experiments, we used oil and various water mixtures of variable density difference ($\Delta\rho$ varying from 20 to 100 kg m^{-3}, $\gamma \sim 25$ mJ m^{-2}) and variable bead diameters (but of constant size in each experiment), resulting into a range of values of B_g from 5×10^{-4} to 10^{-1}. For the permeability gradient experiments, gravity effects were suppressed by using equal density fluids (dibutyl pthalate and water sucrose solutions 11.9 wt. %). An interval of a permeability gradient was created between two regions of uniform permeability (bead size). The gradient was generated by a patient filling of the region with layers of filtered beads of monotonically changing size varying from 800 to 80 μm. The thickness of each layer varied such that the gradient of the bead diameter was constant and equal to B_k. The length of the heterogeneity interval was also variable (5, 10, 15, and 30 cm). However, because of practical limitations, only one decade in B_k [$2.4\times10^{-3}(0.072/30) - 1.44\times10^{-2}(0.072/5)$] was covered in the heterogeneity experiments. The nonwetting fluid (lighter or equally dense fluid) was injected in the direction from top to bottom (or from high to low permeability) in a sample saturated with the wetting fluid (water sucrose solution) at a low constant flow rate (corresponding to a low capillary number $\mathrm{Ca} = \mu q/\gamma \sim 10^{-7}$, where μ is viscosity and q is the displacement velocity). The low-rate restriction was necessary to avoid significant viscous pressure drops. The concentration profile $S_0(x)$ was recorded with the use of an acoustic technique described elsewhere [11], with an accuracy in saturation of 2×10^{-3}. The spatial resolution in the gradient direction was 1 mm, although it is also possible to resolve variations down to 100 μm through a decorrelation method. This high accuracy technique allows for a precise determination of the average front position and of the crossover regime. With the exception of the gravity experiment with $B_g = 0.1$, where a fixed transducer was used and the saturation was monitored as a function of time, all other experiments involved an acoustic scanning device for the determination of the saturation profile. In the permeability gradient case all data were collected near the midpoint of the heterogeneity.

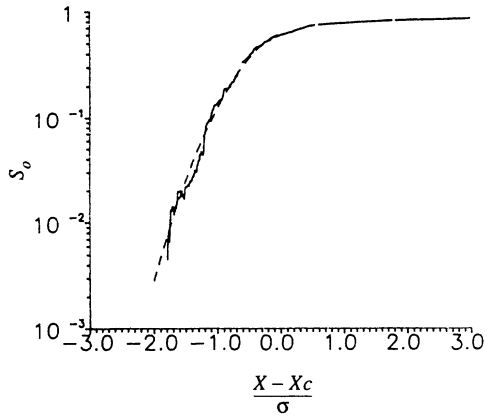

FIG. 2. Experimental profile for invasion percolation in a gradient of hydrostatic pressure ($B_g = 10^{-1}$). Semilogarithmic plot of the nonwetting fluid saturation S_0 versus the reduced space variable. The dashed line is the theoretical prediction (7).

Figure 2 shows the experimental saturation profile plotted versus the reduced position $(x_c - x)/\sigma_{FT}$ for the case of strong gravity effects ($B_g = 10^{-1}$) (where over a thousand experimental points are plotted). The small fluctuations of the concentration are reminiscent of the invasion percolation process (described by the model of the devil staircase [12]). The dashed line through the data is the best fit of the crossover function (4), which is here also extended for positive values of the reduced variable. The fit is excellent and demonstrates the validity of the theory in 3D and over a much wider range [$-3 \le (x_c - x)/\sigma_{FT} \le 1$, $10^{-3} < S_0 \le 1$) than in earlier experiments [5,9] (note the use of a semilogarithmic plot in Fig. 2). Figure 3 shows the corresponding profile for the case of a gradient in permeability ($B_k = 2.4\times10^{-3}$). A good fit with the data is also shown. From these profiles, the front width can be determined as a function of either gravity or permeability Bond numbers, by matching with the theoretical function (4). A plot vs the Bond number

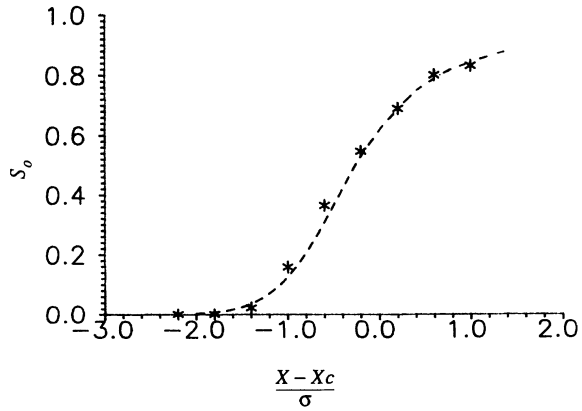

FIG. 3. Experimental profile for invasion percolation in a gradient of permeability ($B_k = 2\times10^{-3}$). Plot of the nonwetting saturation S_0 versus the reduced space variable. The dashed line is the theoretical prediction (4) [or (14)].

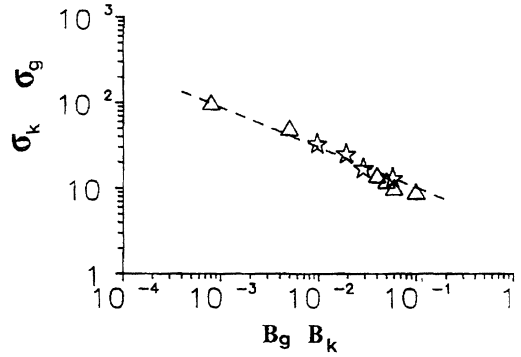

FIG. 4. Log-log plot of the tail width σ (normalized with the local bead size) versus the gravity Bond number B_g (triangles) or the permeability Bond number B_k (stars). The dashed line of slope -0.47 is the theoretical IPG prediction (7).

obtained by this matching is shown in Fig. 4. It should be pointed out that the B_k data required a shift (prefactor adjustment) to coincide with the B_g data; thus the tail for a hydrostatic pressure gradient with $B_g=0.1$ is the same with that for a permeability gradient with $B_k=0.025$ (see also below). The corresponding prefactor may be related to the pore size distribution. The dashed line of slope -0.47 is predicted from (7). We observe that both data sets (B_g and B_k) are consistent with this slope.

The excellent agreement between theory and experiment confirms the validity of the IPG theory for either gravity or permeability gradients in 3D. However, while the case of gravity is very satisfactory, the agreement of the permeability gradient results with (4) and (7) is somewhat unexpected. GP and IPG apply to media of uniform lattice spacing, as is indeed the case with the gravity experiments. In the permeability heterogeneity experiments, however, the spacing varied with the pore size, which is certain to change the scaling. To determine the new scaling, a modification is necessary.

IV. THEORY

To proceed with a theoretical analysis we must stretch the real lattice into a regular lattice of uniform spacing, where GP applies and accordingly transform the probability gradient. Consider a mapping of the real lattice variables $(x,y,z;\sigma)$ to a uniform lattice with variables $(X,Y,Z;\Sigma)$. This lattice has constant spacing (which without loss can be taken as the first bond length $a\bar{r}_1$). In the real lattice, the average pore size at the coordinate location j ($j=1,2,\ldots$) in the direction of the gradient is

$$\bar{r}_{j+1}=\bar{r}_j(1-aB_k)\ , \tag{8}$$

where we made use of the definition of the heterogeneity number $d\bar{r}/dx=-B_k$. We can use (8) to obtain the dependence of $\bar{r}$ with respect to j (or X) in the stretched lattice,

$$\bar{r}_j=\bar{r}_1(1-aB_k)^{j-1},\quad j=1,2,\ldots \tag{9}$$

which shows that although linear with respect to x, the variation with respect to j (or X) is a power law. Using (9) it follows that the coordinate x in the real lattice at location j is

$$x_j=\bar{r}_1\left[\frac{1-(1-aB_k)^{j-1}}{B_k}\right] \tag{10}$$

and in view of $X_j=(j-1)a\bar{r}_1$, real (x) and stretched (X) lattice coordinates are related via

$$x=\frac{\bar{r}_1}{B_k}[1-(1-aB_k)^{X/a\bar{r}_1}]\ . \tag{11}$$

We can now apply gradient percolation theory to the uniform lattice problem (always recalling that the probability p varies with x) to obtain the result

$$\Sigma\sim\xi(X_c\pm\Sigma)\ , \tag{12}$$

where $\xi\sim a\bar{r}_1|p-p_c|^{-\nu}$. Inherent to (12) is the assumption that gradient percolation results remain valid even when the lattice size changes in the transverse to the gradient direction ($y,z\rightarrow Y,Z$), an assumption which was actually confirmed numerically. We may then proceed by recalling that $p-p_c=-B_k(x-x_c)/\lambda$ and $\sigma\sim\Sigma(dx/dX)_c$, where x and X are related through (11), to arrive at the final result

$$\left[\frac{\sigma}{\lambda}\right]^{1+\nu}\sim B_k^{-(\nu+1)}\left[1-\frac{x_cB_k}{\bar{r}_1}\right]\ln\left[\frac{1}{1-aB_k}\right]\left[\frac{\bar{r}_1}{\lambda}\right]\ . \tag{13}$$

This more general scaling is different from the classical (7), which, however, it approaches in the small B_k limit. In fact, the above shows that σ decreases as x_c (or time) increases. How can the new scaling be reconciled with the experimental findings? Before we proceed to an answer, we first present a numerical confirmation of the theory.

To simulate IP in a permeability gradient we modeled the porous medium as a square or cubic lattice of nodes (pores) connected by bonds of size $200\times NX$ (where NX ranged from 220 to 2250) or $55\times55\times NX$ (although data were also collected for $32\times32\times NX$) (where NX ranged from 150 to 900), respectively. The bond size was distributed uniformly with mean values assigned according to (9) and with a constant λ, thus the lattice has a monotonically changing (decreasing if $B_k>0$) spacing. The theoretical prediction (13) was tested by plotting the values of σ for different times and Bond numbers in the appropriate log-log plot. 2D results shown in Fig. 5 have a computed slope of 0.429, in excellent agreement with the theoretical prediction of $1/(1+\nu)=0.4285$. Good results are also shown for the 3D simulations (where the slope is 0.545 compared to the expected 0.532) (Fig. 6). The scatter of the data was found to diminish and the agreement with the theory becomes better as the network cross-section increases.

The occupied fraction p_f', which is related to the experimental saturation via $p_f'=S_0/p$, can be also determined. We proceed as follows: For the uniform spacing lattice (where real space is not yet involved) we expect (4) to ap-

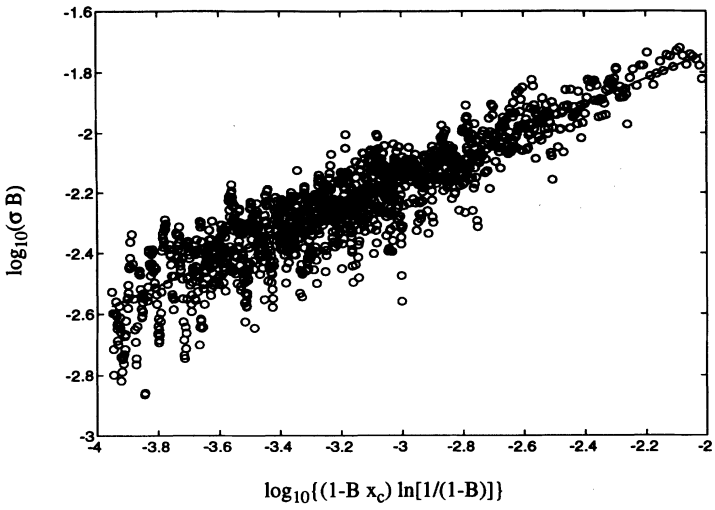

FIG. 5. Scaling of the front width σ vs the permeability gradient Bond number B_k and front location x_c in 2D lattices of decreasing spacing (σ and x_c are normalized with $\bar{r}_1$). The computed slope 0.429 agrees well with the theoretical value 0.4285. A total of 1410 points are plotted.

ply. Incidentally, we should note that (4) was derived only for GP [8]. In our simulations, we found that when an invasion problem is involved, the numerical results can fit to the scaling function Π_f, but only after a stretch of the reduced variable. This was found necessary in both gravity and heterogeneity cases. Although not explicitly stated in Ref. [5], we assume that a similar stretching was also done there. The final result for the uniform lattice problem is

$$p_f' \sim \Sigma^{-\beta/\nu} \Pi_f \left[\frac{p - p_c}{c(\Sigma/l)^{-1/\nu}} \right], \tag{14}$$

where the constant c was found to be of order 3 in both cases. To convert to the real lattice, we substitute the previous relations between real and lattice variables to obtain

$$p_f' \sim \left[B_k \frac{\sigma}{\lambda} \right]^{\beta} \Pi_f \left[\frac{x - x_c}{c\sigma} \right]. \tag{15}$$

Although Eq. (15) is different from (4), the scaling of the spatial variation of saturation is the same in both equations, thus allowing for σ to be directly inferred. (Note that the factor c remains constant as the Bond number varies.)

The agreement of the permeability gradient experimental results with the theoretical slope 0.47 can now be interpreted. As pointed out above, the heterogeneity results were collected at the midpoint of the heterogeneity region, which by construction has a constant mean pore size for any B_k. Since in (13) $1-(x_c B_k/\bar{r}_1)$ also represents a normalized pore size, this implies a fixed value for the product $x_c B_k$. Substitution in (13) and using $B_k \ll 1$ in the expansion of the logarithm yields $\sigma^{1+\nu} \sim B_k^{-\nu}$, which is the scaling of the standard IPG. The same interpretation holds for the saturation profile. On the other hand, for arbitrary, and variable, x_c locations the more general scaling (13) should be obeyed. The inadequacy of the direct GP relationship $\sigma/\bar{r}_c \sim B_k^{-\nu/1+\nu}$ to describe the present heterogeneity case, where the lattice spacing is variable, was demonstrated by replotting the 3D numerical data corresponding to Fig. 6. The results are shown in Fig. 7. We see that the data are widely scattered and do not suggest the theoretical straight line

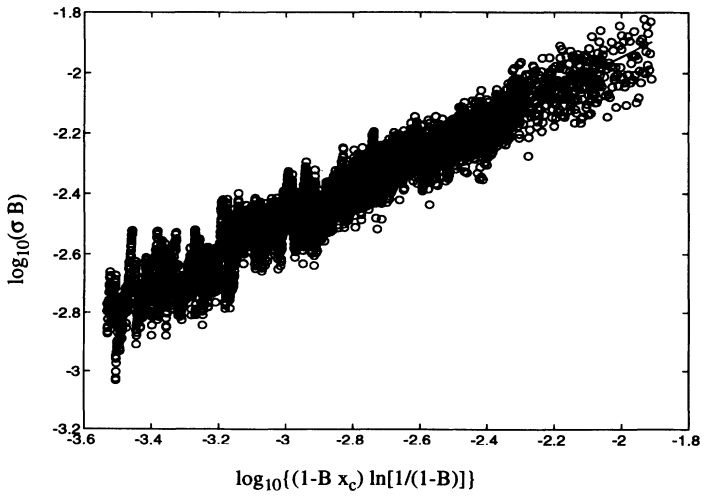

FIG. 6. Scaling of tail width σ_{FT} vs permeability gradient Bond number B_k and front location x_c in 3D lattices of decreasing spacing (σ_{FT} and x_c are normalized with $\bar{r}_1$). The computed slope is 0.545 compared to the theoretical value of 0.532. A total of 5916 points are plotted.

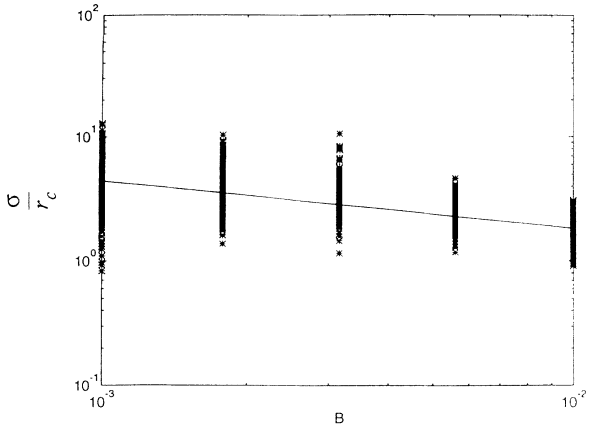

FIG. 7. Log-log plot of the normalized tail width σ/r_c vs the permeability gradient Bond number B_k in 3D lattices of decreasing spacing. An attempt to fit the data with the unmodified GP equation (7) gives a straight-line slope of -0.38 compared to the theoretical value of -0.47.

of (7). In fact, the best fit in a log-log plot gives a straight line slope of -0.38 compared to the expected -0.47.

V. CONCLUSIONS

In conclusion, it was shown that IPG describes slow drainage in either homogeneous media involving hydrostatic gradients or in heterogeneous media involving permeability gradients. For the former case, 3D experiments confirmed and extended the validity of the theory. For the latter case, the conjecture was verified experimentally in 3D glass bead packs of varying size, where a modified IPG theory was also developed. Theory and experiments were also confirmed with numerical simulation.

The experimental data clearly demonstrated the equivalence between hydrostatic pressure and permeability gradients, subject to the above modification, wherever appropriate. Theory and experiments can be extended to cases where both effects are acting: when both gravity and permeability are stabilizing ($B_g > 0$ and $B_k > 0$), the front width would scale with the overall Bond number. So is the case when one of the two effects is destabilizing,

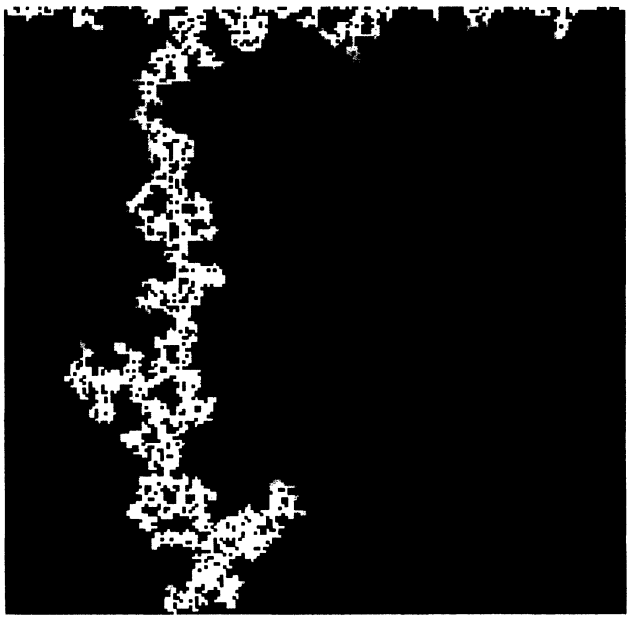

FIG. 8. Numerical simulation of 2D capillary fingering in a permeability gradient ($B_k = -0.001$).

but still the overall Bond number is positive $B_g + mB_k > 0$, where the proportionality factor m is required to collapse both permeability and heterogeneity data. When the overall Bond number is negative, the result would be capillary heterogeneity fingering. A similar regime involving gravity-driven fingering was described in Ref. [6], where $B_g < 0$ and $B_k = 0$. A numerical simulation of this regime for the heterogeneity case is shown in Fig. 8, where the permeability is increasing in the direction of displacement ($B_k < 0$). The analysis of this regime is currently in progress.

ACKNOWLEDGMENTS

The work of M.C., N.R., and D.S. was supported by GDR CNRS Physique des Milieux Heterogenes Complexes. B.X. and Y.C.Y. were partly supported by DOE Contract No. DE-FG22-90BC14600. The collaboration was facilitated by NATO Grant No. CRG 901053. All these sources of support are gratefully acknowledged.

[1] R. Lenormand, J. Phys. Condens. Matter **2**, SA79 (1990).
[2] L. Patterson, Phys. Rev. Lett. **52**, 1621 (1984); T. A. Witten and L. M. Sander, Phys. Rev. B **27**, 5686 (1983).
[3] D. Wilkinson and J. F. Willemsen, J. Phys. A **16**, 3365 (1983).
[4] J. Feder, Fractals (Plenum, New York, 1988).
[5] J. P. Hulin, E. Clément, C. Baudet, J. F. Gouyet, and M. Rosso, Phys. Rev. Lett. **61**, 333 (1988); J. F. Gouyet, M. Rosso, E. Clément, C. Baudet, and J. P. Hulin, in *Hydrodynamics of Dispersed Media,* edited by J. P. Hulin, A. M. Cazabat, E. Guyon, and F. Carmona (Elsevier, New York, 1990), p. 179.
[6] V. Frette, J. Feder, T. Jossang, and P. Meakin, Phys. Rev. Lett. **68**, 3164 (1992).
[7] D. Wilkinson, Phys. Rev. A **30**, 520 (1984).
[8] B. Sapoval, M. Rosso, and J. F. Gouyet, J. Phys. (Paris) Lett. **46**, L149 (1985); J. F. Gouyet, M. Rosso, and B. Sapoval, Phys. Rev. B **37**, 1832 (1988).
[9] A. Birovljev, L. Furuberg, J. Feder, T. Jossang, K. J. Maloy, and A. Aharony, Phys. Rev. Lett. **67**, 584 (1991).

[10] J. Chang and Y. C. Yortsos, Transp. Porous Media **5**, 399 (1990); J. Chang and Y. C. Yortsos, Soc. Pet. Eng. Reserv. Eng. **7**, 285 (1992); M. Chaouche, N. Rakotomalala, D. Salin, and Y. C. Yortsos, Europhys. Lett. **21**, 79 (1993); A. K. Stubos, C. Satik, and Y. C. Yortsos, Int. J. Heat Mass Transfer **36**, 967 (1993).

[11] J.-C. Bacri, M. Hoyos, R. Lenormand, N. Rakotomalala, A. Soucemariadin, and D. Salin, J. Phys. III **1**, 1455 (1991); J.-C. Bacri and D. Salin, Geophys. Res. Lett. **13**, 326 (1986).

[12] A. J. Katz and A. H. Thompson, Phys. Rev. B **34**, 8175 (1987).